


Cycle Flux Ranking of Network Analysis in Quantum Thermal Devices

Luqin Wang¹, Zi Wang¹, Chen Wang^{2,*} and Jie Ren^{1,†}

¹Center for Phononics and Thermal Energy Science, China-EU Joint Lab on Nanophononics, Shanghai Key Laboratory of Special Artificial Microstructure Materials and Technology, School of Physics Sciences and Engineering, Tongji University, Shanghai 200092, China

²Department of Physics, Zhejiang Normal University, Jinhua 321004, Zhejiang, People's Republic of China

 (Received 15 July 2021; revised 8 December 2021; accepted 19 January 2022; published 8 February 2022)

Manipulating quantum thermal transport relies on uncovering the principle working cycles of quantum devices. Here we introduce the cycle flux ranking of network analysis to nonequilibrium thermal devices characterized as a quantum-transition network. To excavate the principal mechanism out of complex transport behaviors, we decompose the network into cycle trajectories, collect the cycle fluxes by algebraic graph theory, and select top-ranked cycle fluxes, i.e., the cycle trajectories with highest probabilities. We exemplify the cycle flux ranking in typical quantum device models, e.g., a thermal-drag spin-Seebeck pump and a quantum thermal transistor. Top-ranked cycle trajectories indeed elucidate the principal working mechanisms. Therefore, cycle flux ranking provides an alternative perspective that naturally describes the working cycle corresponding to the main functionality of quantum thermal devices, which would further guide the device optimization with desired performance.

DOI: [10.1103/PhysRevLett.128.067701](https://doi.org/10.1103/PhysRevLett.128.067701)

Introduction.—Harnessing heat and information at the nanoscale constitutes one active frontier of functional thermal devices [1–11], in analogy with modern electronics [12]. The ubiquitous quantum effects further fertilize the routes toward quantum thermal transport and enhance the flexibility of heat management [13–16]. Various quantum thermal devices are attracting tremendous attention together with both theoretical modelings [17–29] and practical realizations [30–33], paving the avenue for the design of on-chip thermal devices.

Meanwhile, network theory becomes an important method to describe the quantum transport [34–41], where nonequilibrium effects of external dissipative reservoirs can be incorporated into the edge weights of the directed network of state transitions [42]. In general, the network analysis of nonequilibrium transport can be established by cycle decomposition in the graph theory [43–45]. This leads to a flurry of inspiring works. In particular, Nitzan *et al.* investigated quantum transport control from the cycle viewpoint in both photovoltaics' state networks [46,47] and electrothermal networks [48–50]. Zhang and Wang studied the antisymmetric driving force via curl flux in the donor-acceptor model [51]. While considering the dynamical driving, Jarzynski and co-worker's [52], and Chernyak and Sinitsyn [53], together with subsequent research [54–56], revealed and emphasized the peculiar role played by cycle graphs in general no-pumping theorems. Furthermore, as a kind of quantum machine, the full functioning of a quantum thermal device fundamentally requires completing cycles in the state space, the same as thermodynamic cycles in quantum heat engines [57–60] and quantum refrigerators

[61–63]. Therefore, the cycle analysis of network theory should be a powerful approach to explore the detailed mechanism of dissipative quantum thermal devices.

In this Letter, we propose an efficient ranking scheme to explore thermal transport in quantum thermal devices. By mapping quantum thermal devices into networks of quantum state transitions, one can decompose the transition network into cycle trajectories. Hence, nonequilibrium quantum transports can be microscopically represented by cycle trajectories that are formed of self-avoiding closed quantum transitions. Such cycle trajectories are the key ingredients affecting the performance of quantum thermal devices [48–50,64–67]. However, the formidable complexity is dictated by the huge number of cycle trajectories, composed of massive quantum states and transitions among them. This inspires us to explore the complex transport behaviors from the top-ranked cycle trajectories with largest occurring probabilities, i.e., top-ranked cycle fluxes.

Benefiting from algebraic graph theory, all cycle fluxes can be calculated and ranked efficiently. By selecting the top-ranked cycle trajectories, we could surmount the challenge caused by huge dimensional parameter space, to genuinely grasp the physical essence of the multifunctional quantum devices. Concretely, we utilize two typical quantum device models, thermal-drag spin-Seebeck pump and quantum thermal switch, to demonstrate the power of cycle flux ranking of network analysis.

Connecting quantum transport with cycle flux ranking.—The dissipative dynamics of quantum systems are conventionally described by the quantum master equation in Lindblad form [68,69]

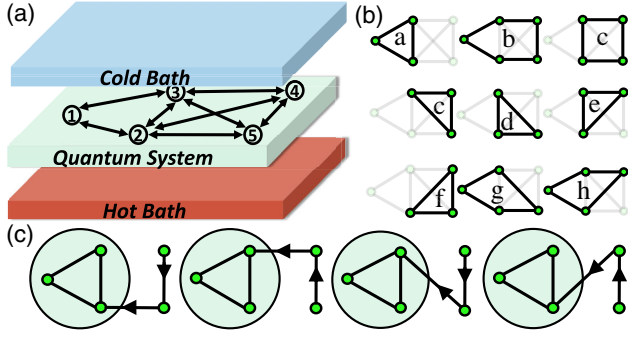


FIG. 1. Mapping dissipative quantum devices into networks. (a) Schematic of a transition network for quantum thermal transport under nonequilibrium conditions. (b) All undirected cycle graphs contained in the transition network. (c) All the spanning trees rooted on (every edge is oriented toward) cycle $C_{1 \rightarrow 2 \rightarrow 3 \rightarrow 1}$.

$$\frac{d\rho_s(t)}{dt} = i[\rho_s, H_s] + \sum_v \mathcal{D}_v[\rho_s], \quad (1)$$

where ρ_s is the reduced density matrix, and $\mathcal{D}_v[\rho_s]$ is the Lindblad superoperator describing the dissipation induced by the v th thermal reservoir. The off-diagonal coherence ρ_{ij} vanishes when approaching steady states. Also, it was pointed out by Zurek [70] that open quantum systems interacting with a reservoir Hamiltonian can be cast into a diagonal form. Moreover, Wu and Cao showed that, by applying higher-order kinetic expansion, the quantum dissipative dynamics with coherence can be mapped into kinetic networks [42]. Without loss of generality, the quantum Lindblad equation can be reduced into a Pauli master equation: $\dot{\rho}_{ii} = -\sum_j L_{ij}\rho_{jj}$, where ρ_{ii} denotes the probability to observe the system in state $|i\rangle$ (see Supplemental Material, Sec. I [71]), and $L_{ij} = -\sum_v k_{j,i}^v + \delta_{ij} \sum_{v,m} k_{j,m}^v$ is the Laplacian transition matrix describing the open dissipative system under nonequilibrium conditions, with forward (backward) transition rate $k_{j,i}^v$ ($k_{i,j}^v$) induced by the v th reservoir. Therefore, the dissipative quantum dynamics is represented by a network with Laplacian matrix element L_{ij} , as depicted in Fig. 1(a), where the vertices denote the quantum states and the weighted edges denote the transitions from $|j\rangle$ to $|i\rangle$ with positive rates.

Specifically, the network can be represented on the basis of cycle trajectories, and the edge flux can be decomposed into cycle fluxes $J_{i \rightarrow j} = \sum_C J_{C_+} - J_{C_-}$, where the summation is over all cycle trajectories C that contain the edge ($i \rightarrow j$), with subscript $+$ ($-$) for the forward (backward) cycle along (opposite to) the $|i\rangle \rightarrow |j\rangle$ direction. For example, Fig. 1(b) lists all cycle trajectories of the network, and the net edge flux $J_{3 \rightarrow 2} = (J_{a_+} + J_{c_+} + J_{d_+} + J_{e_+}) - (J_{a_-} + J_{c_-} + J_{d_-} + J_{e_-})$. The concept of cycle fluxes, pioneered by Hill *et al.* [74,75] and developed by

Kohler and Vollmerhaus [76] and Schnakenberg [43], can be intuitively understood as the cycle frequency, quantifying how many rounds the state can transit through one complete cycle per unit time, and have been widely carried out in describing biochemical systems [77–81].

The cycle flux of the cycle trajectory C_{\pm} is formulated as $J_{C_{\pm}} = \Pi_{C_{\pm}} \Sigma_C / \Sigma$ [74], where $\Pi_{C_{\pm}}$ is the weight of the cycle trajectory C_{\pm} defined as the product of transition rates along cycle C , Σ_C is the sum of weights of spanning trees that are rooted on the cycle C , and Σ is the sum of weights of spanning trees rooted on every individual state. In practice, it will be challenging to count the vast number of spanning trees rooted on different vertices. Nevertheless, we surmount this difficulty by using the generalized matrix-tree theorem in algebraic graph theory. The introduction of algebraic graph theory to investigate nonequilibrium transport in thermodynamic networks was already reported [64–66]. However, here the generalized matrix-tree theorem states that the principal minor of Laplacian L of the weighted graph has the determinant $\det(L[C; C])$, by deleting rows and columns $i \in C$ from L , which equals the sum of weights of directed spanning trees rooted on the cycle C , i.e., $\det(L[C; C]) = \Sigma_C$. This directly leads to a simple algebraic expression of cycle flux,

$$J_{C_{\pm}} = \Pi_{C_{\pm}} \frac{\det(L[C; C])}{\sum_i \det(L[i; i])}, \quad (2)$$

with $\sum_i \det(L[i; i]) = \Sigma$. This algebraic expression of cycle flux can be intuitively interpreted as that [79] the directed flow of weighted edges on spanning trees toward a cycle is tightly related with the occurring frequencies of the cycle trajectory. The flow of directed edges toward the state increases its chance of occupation. The alternative mathematical proof concerning the Markov chain can be found in Ref. [82]. In Fig. 1(c), we show the four spanning trees rooted on cycle $C_{1 \rightarrow 2 \rightarrow 3 \rightarrow 1}$, the weight sum of which leads to the factor $\det(L[1, 2, 3; 1, 2, 3])$. By multiplying the weight of the cycle itself $\Pi_{1 \rightarrow 2 \rightarrow 3 \rightarrow 1} = k_{1,2} k_{2,3} k_{3,1}$ upon normalizing a common factor $\sum_{i=1}^5 \det(L[i; i])$, the cycle flux $J_{C_{1 \rightarrow 2 \rightarrow 3 \rightarrow 1}}$ can be readily calculated. In addition, $\det(L[1, 2, 3; 1, 2, 3])$ is identical to $\det(L'[d, d])$ in a new graph L' , which formed by merging vertex $\{1, 2, 3\}$ into a new vertex d in the original graph L represented by the big green shadow circle. Hence, following the same procedure, we can calculate the cycle fluxes of all the cycle trajectories as listed in Fig. 1(b) and efficiently rank out the top-ranked cycle fluxes. We note that the advantage of the cycle flux ranking is supposed to be enhanced as the number of quantum states embedded in the quantum network further increases. However, the ranking scheme, inherited from the matrix analysis, may become less efficient in huge Hilbert-space dimension limit.

In what follows, we apply the above ranking scheme to analyze two typical transport models of quantum devices:

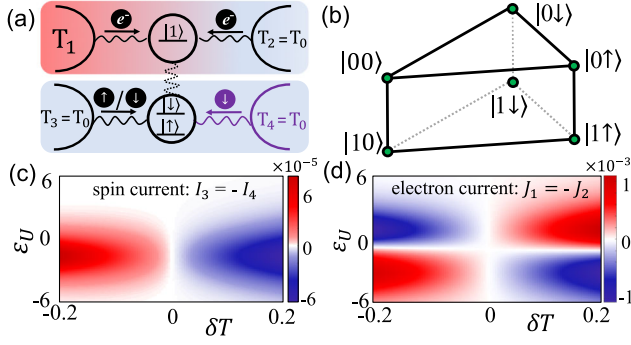


FIG. 2. The thermal-drag spin-Seebeck pump. (a) Scheme of thermal-drag spin-Seebeck pump in hybrid dot structures. The upper dot is coupled with two spinless electron reservoirs. The lower dot is coupled with a spinful electron reservoir (left) and a magnon bath (right). The two dots are Coulomb coupled. (b) Quantum-transition network in state space. (c),(d) Spin current I_3 ($-I_4$) and electron current J_1 ($-J_2$) by tuning $\delta T = T_1 - T_0$ and ε_U , respectively, where $I_{i=3,4}$ ($J_{i=1,2}$) is the net spin (electron) current flowing from reservoir i into the center system. Other parameters are $\varepsilon_{L\downarrow} = -\varepsilon_{L\uparrow} = 1$, $U = 3$, and $T_2 = T_3 = T_4 = T_0 = 1$. The calculation details are in the Supplemental Material, Sec. II [71].

thermal-drag spin-Seebeck pump and quantum thermal transistor. Results demonstrate the advantages of the efficient ranking scheme that the top-ranked cycle fluxes indeed elucidate their principal working mechanisms.

Thermal-drag spin-Seebeck pump: The first hybrid quantum model is illustrated in Fig. 2(a). The upper dot, with two states $|\phi_U\rangle = \{|0\rangle, |1\rangle\}$, is connected with two spinless electron reservoirs: $V_U = t_U \sum_{k,v=\{1,2\}} c_{U,v,k}^\dagger d_{U,v} + \text{H.c.}$ The lower dot, with three states $|\phi_L\rangle = \{|0\rangle, |\uparrow\rangle, |\downarrow\rangle\}$, is connected with both a left-side spinful electron reservoir and a right-side magnon bath [83]: $V_L = t_L \sum_{k,\sigma=\{\uparrow,\downarrow\}} c_{L,\sigma,k}^\dagger d_{L,\sigma} + \gamma \sum_q b_q^\dagger d_{L,\uparrow}^\dagger d_{L,\downarrow} + \text{H.c.}$ c_k^\dagger (c_k) and b_q^\dagger (b_q) are creation (annihilation) operators in an electron reservoir with momentum k and in a magnon bath with momentum q , respectively. The upper and lower dots are Coulomb coupled with each other, with the Hamiltonian

$$H_s = \sum_{v=U,L} \varepsilon_v \hat{n}_v + U \hat{n}_L \hat{n}_U, \quad (3)$$

where $\hat{n}_U = d_U^\dagger d_U$ and $\hat{n}_L = \sum_\sigma d_{L,\sigma}^\dagger d_{L,\sigma}$ are the number operators of two dots. Although with the Coulomb energy U coupling the upper and lower subsystems, the electron transport is only across the upper one, while the spin transport occurs merely through the lower one. Under the eigenstate basis $|\phi_U \phi_L\rangle$, the corresponding quantum-transition network is depicted in Fig. 2(b).

An intriguing phenomenon emerges in which a nonzero spin current across the lower isothermal subsystem is pumped by the nonzero thermal bias $\delta T = T_1 - T_0$ across

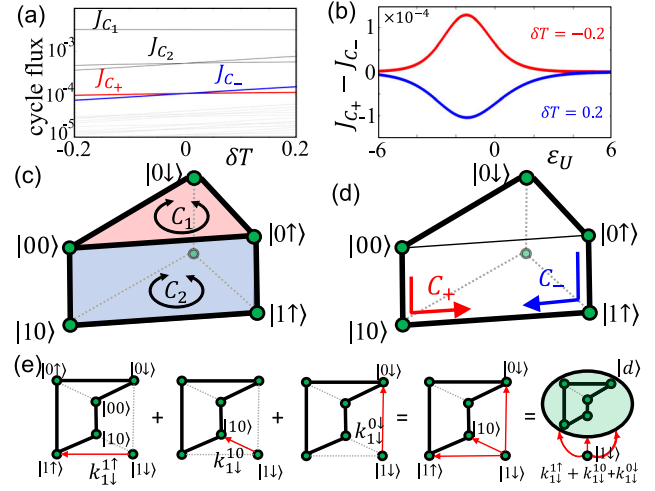


FIG. 3. Cycle flux ranking analysis of the thermal-drag spin-Seebeck pump. (a) Top-ranked cycle fluxes at $\varepsilon_U = 1$. The dominant cycle fluxes are represented by the bold red (light) and blue (dark) lines. (b) The net cycle flux $J_{C_+} - J_{C_-}$ as a function of ε_U for $\delta T = -0.2$ and 0.2 , respectively. (c) The first- (C_1) and second-ranked (C_2) paired cycle trajectories. (d) The third-ranked paired cycle trajectories (C_\pm) are represented by the bold lines that dominate the spin-Seebeck pump at $\varepsilon_U = 1$. (e) The spanning tree analysis of the cycle trajectory (C_\pm) based on the generalized matrix-tree theorem in algebraic graph theory.

the upper subsystem, as shown in Fig. 2(c). By tuning ε_U , the thermal generated electron current in the upper subsystem will vanish and reverse due to the effective particle-hole symmetry, as shown in Fig. 2(d). Yet, the thermal-excited spin-Seebeck current in the lower subsystem still reaches maximum near ε_U of vanishing electron current. This result provides a strong evidence suggesting nontrivial mechanism beyond normal Coulomb drag effect caused by drifted electron current.

To show the power of an efficient ranking scheme in excavating the working cycle in the four-terminal spin pump quantum thermal device, we decompose the network of the spin-Seebeck process into a complete set of cycle trajectories. There are in total 28 paired cycle trajectories based on Fig. 2(b). After the efficient ranking with Eq. (2), the top-ranked cycle fluxes are plotted in Fig. 3(a). Then, we select the main working cycles underlying the thermally driven spin pump effect. Specifically, the first-ranked paired cycle trajectory is illustrated in Fig. 3(c) (top surface marked with C_1): $|00\rangle \rightarrow |0\uparrow\rangle \rightarrow |0\downarrow\rangle \rightarrow |00\rangle$ and vice versa. Because of the vanishing of affinity along these cycle trajectories, i.e., $(k_{00}^{0\uparrow} k_{0\uparrow}^{0\downarrow} k_{0\downarrow}^{00} / k_{00}^{0\downarrow} k_{0\downarrow}^{0\uparrow} k_{0\uparrow}^{00}) = 1$ ($k_{a,b}^c \equiv k_{a,b,c}$, see Table II in the Supplemental Material [71]), the first-ranked paired cycles are futile to the thermal-driven spin pump. As for the second-ranked paired cycles with the trajectory shown in Fig. 3(c) (front surface marked with C_2), i.e., $|00\rangle \leftrightarrow |10\rangle \leftrightarrow |1\uparrow\rangle \leftrightarrow |0\uparrow\rangle \leftrightarrow |00\rangle$, the spin does not flip, which also makes no contribution to the spin pump.

The third-ranked paired cycle trajectories in Fig. 3(d), i.e., C_+ and C_- , are unraveled to dominate the spin current generation [see Figs. 2(d) and 3(b)]. We first exemplify the spanning trees of the cycle trajectory, e.g., C_{\pm} , based on the generalized matrix-tree theorem in algebraic graph theory in Fig. 3(e). The first three spanning trees denote three transitions, respectively. By deleting corresponding columns and rows involved in C_{\pm} from the Laplacian matrix, we get the determination of the resultant matrix $k_{1\downarrow}^{1\uparrow} + k_{1\downarrow}^{10} + k_{1\downarrow}^{0\downarrow}$, which is described by the fourth tree configuration. Meanwhile, by merging the cycle trajectory (C_{\pm}) into a new vertex d , we obtain a new graph shown in the fifth configuration, and deleting the d th column and row is identical to the former situation [71]. Then, we illustrate the five dynamical steps of the forward cycle trajectory C_+ as follows: Starting from $|00\rangle$, the system transits sequentially into $|10\rangle$ (one electron jumps into the upper dot), $|1\uparrow\rangle$ (one spin-up electron tunnels from reservoir 3 into the lower dot), $|0\uparrow\rangle$ (the upper electron jumps out), $|0\downarrow\rangle$ (the lower electron becomes spin-down by absorbing one magnon), and finally back to $|00\rangle$ (the lower spin-down electron jumps to reservoir 3). In particular, along the cycle trajectory C_+ , a spin-up electron tunnels into the lower dot from reservoir 3 ($|00\rangle \rightarrow |0\uparrow\rangle$), then flips to the spin-down state ($|0\uparrow\rangle \rightarrow |0\downarrow\rangle$) by absorbing one magnon, and finally tunnels into reservoir 4 ($|0\downarrow\rangle \rightarrow |00\rangle$). After one complete cycle trajectory C_+ , an integer spin 1 is transferred from the left electron reservoir to the right magnon bath. Similarly, the backward cycle trajectory C_- gives the reverse process. These two cyclic processes cooperatively contribute to the thermal-drag spin-Seebeck pump effect. Moreover, with the opposite sign of δT , the competition of weights $\Pi_{C_{\pm}}$ in Eq. (2) between main cycle trajectories (C_+ and C_-) leads to the reversal of the spin current, e.g., in Fig. 3(b).

We further apply $J_{C_{\pm}}$ to analyze the spin-Seebeck pump effect in the linear response regime. Interestingly, we can readily obtain the forward-backward ratio of $J_{C_{\pm}}$,

$$\frac{J_{C_+}}{J_{C_-}} = \frac{\Pi_{C_+}}{\Pi_{C_-}} \approx 1 - \frac{U\delta T}{2T_0^2}. \quad (4)$$

This clearly demonstrates that the thermal bias (δT) in the upper subsystem and the Coulomb repulsion (U) between upper and lower subsystems synergistically determine the emergence of the spin-Seebeck pump effect in the lower subsystem. Furthermore, changing the sign of δT would reverse the net main cycle flux $J_{C_+} - J_{C_-}$ and spin-Seebeck current $I_3 \propto J_{C_+} - J_{C_-}$, as shown in Fig. 3(b). In contrast, for a given δT , changing ϵ_U does not reverse the main cycle fluxes, although the electron current through the upper subsystem is reversed. Therefore, nonzero spin current generation (cycle flux $J_{C_+} - J_{C_-}$) at vanishing electron current regime in the upper subsystem further clarifies the working mechanism as the thermal-drag spin-Seebeck pump effect.

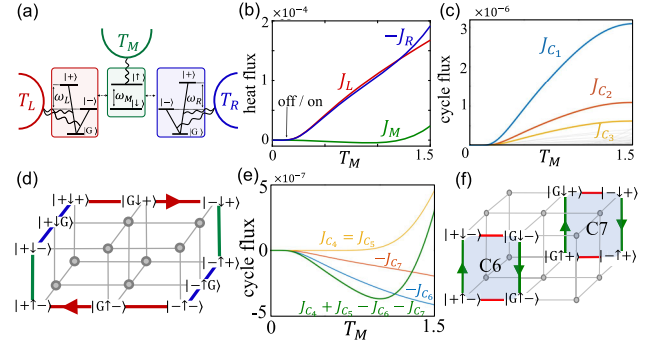


FIG. 4. Cycle flux ranking in quantum thermal transistor. (a) Schematic of the quantum thermal transistor, which is composed of the qutrit-qubit-qutrit system, individually coupled to one thermal bath denoted by a half circle with T_v ($v = L, M, R$). (b) Heat currents from left to right as a function of T_M . (c) Top-ranked cycle fluxes as a function of T_M . (d) The first-ranked cycle trajectory C_1 embedding in the state network. (e) Top-ranked cycle fluxes contributed to J_M . (f) Cycle trajectories for C_6 and C_7 . The other parameters are $\omega_{L,M,R} = 1$, $\omega_{LM} = \omega_{MR} = 10$, $\omega_{LR} = 0$, $\omega_{0,L(R)} = 3$, $T_L = 2.5$, and $T_R = 0.2$. See the calculation detail in the Supplemental Material, Sec. III [71].

We note that the novelty of the thermal-drag spin-Seebeck pump has three manifolds: (i) From the model perspective, the present four-terminal quantum system includes the upper and lower subsystems. It is known that these two individual subsystems have been extensively investigated [72,83–85]. However, the combination of these two nonequilibrium systems to analyze the spin current generation is lacking exploration. (ii) From the spin-Seebeck effect perspective, the current work based on the four-terminal setup unravels the thermal-drag induced robust spin-Seebeck pump, rather not the conventional Coulomb-drag Seebeck effect [86,87]. (iii) From the technique perspective, we introduce the cycle flux ranking scheme to efficiently capture the main working cycles, which dominates the spin-Seebeck pump process.

Quantum thermal transistor: We then apply the cycle flux ranking to investigate typical functionalities of the second quantum device model, e.g., quantum thermal switch and negative differential thermal conductance (NDTC). Figure 4(a) exhibits a hybrid qutrit-qubit-qutrit system connected to three individual boson baths with the Hamiltonian $H_{b,u=\{L,M,R\}} = \sum_k \omega_{u,k} a_{u,k}^\dagger a_{u,k}$. The left (right) V -type qutrit is coupled with the photon bath via $V_{v=\{L,R\}} = \sum_k (g_{v,k}^+ a_{v,k}^\dagger |G_v\rangle \langle +_v| + g_{v,k}^- a_{v,k}^\dagger |G_v\rangle \langle -_v|) + \text{H.c.}$, and the middle one is coupled with a phonon bath via $V_M = \sum_k g_{M,k} (a_{M,k}^\dagger \sigma_M^- + a_{M,k} \sigma_M^+)$, where $g_{u,k}$ is the coupling strength [73]. The hybrid central Hamiltonian takes the variant of Ref. [20] as

$$H_s = \sum_{u=L,M,R} \frac{\omega_u}{2} \sigma_u^z + \sum_{v=L,R} \left(\frac{\omega_{vM}}{2} S_v^z \sigma_M^z + \omega_{0,v} S_v^0 \right), \quad (5)$$

where σ_M^z is the middle qubit Pauli matrix, and the left and right qutrits are $S_v^z = |+_v\rangle\langle+_v| - |-_v\rangle\langle-_v|$ and $S_v^0 = |+_v\rangle\langle+_v| + |-_v\rangle\langle-_v|$, with $v = L, R$.

Figure 4(b) exhibits the quantum thermal switch effect by tuning the middle gating temperature T_M . When T_M is sufficiently low, three heat currents are suppressed and the system is at the *off* state. As T_M exceeds a threshold value, the source and drain heat currents J_L and $-J_R$ are dramatically enhanced, whereas the gating heat current J_M is still negligible [88]. As such, the system switches to the *on* state.

Based on Eq. (2), we enumerate all cycle trajectories to realize an efficient flux ranking scheme. By analyzing the trajectories of top-ranked cycle fluxes, it is straightforward to know that the flux J_{C_1} in Fig. 4(c) shows the main contribution to the thermal switch effect. As the principal working cycle trajectory in Fig. 4(d), C_1 is indispensable to J_L and J_R , which, however, becomes irrelevant with J_M . Along the trajectory C_1 , the heat flow (J_M) via the paths $|\downarrow+\rangle \rightarrow |-\uparrow+\rangle$ and $|+\uparrow-\rangle \rightarrow |+\downarrow-\rangle$ is completely canceled. Therefore, during this cycle trajectory, no heat exchanges between the hybrid system and the middle thermal bath. Moreover, the fluxes J_{C_2} and J_{C_3} , similar with J_{C_1} , also show the secondary contribution to such thermal switch effect. Further dissecting J_{C_1} , we find that the switch threshold relies on a principal factor ω_M/T_M , which guides us to inverse design the quantum thermal switch with tunable threshold [71].

Meanwhile, the hybrid system also exhibits the NDTC of J_M , which stems from the cycle flux competition. Looking into the cycle fluxes listed in Fig. 4(e), we identify that the cycle fluxes of C_6 and C_7 dominate the NDTC of J_M , flowing from the middle reservoir into the system, of which the cycle trajectories are illustrated in Fig. 4(f). During the complete cycle trajectory $C_6(C_7)$, the right qutrit keeps frozen at state $|-\rangle(|+\rangle)$, which describes a simplified working picture that the reduced system absorbs energy from the left reservoir and emits energy into the middle bath by qubit flipping. These two corresponding cycle fluxes J_{C_6} and J_{C_7} , in contrast to J_{C_4} and J_{C_5} , contribute negatively to J_M . Then, by increasing T_M , although the thermal bias $T_L - T_M$ becomes smaller, the middle qubit flipping process is easily thermally excited by the middle reservoir. This process dramatically enhances the quantum thermal transport, i.e., $\partial J_M / \partial T_M < 0$.

Conclusion.—By mapping the dissipative quantum thermal devices into networks of quantum state transitions, we have decomposed the transition network into cycle trajectories and showed the advantage of the cycle flux ranking in nonequilibrium thermal transport. With the help of an efficient ranking scheme, we have demonstrated that the top-ranked cycle fluxes genuinely grasp the principal mechanism out of complex transport features, such as thermal-drag spin-Seebeck pump, quantum thermal switch, and NDTC. Top-ranked cycle flux analysis provides

researchers an alternative viewpoint to investigate quantum thermal transport and would promote the optimization of multifunctional quantum thermal devices.

The work is supported by the National Natural Science Foundation of China (No. 11935010, No. 11775159, and No. 11704093) and the Opening Project of Shanghai Key Laboratory of Special Artificial Microstructure Materials and Technology.

*wangchenyifang@gmail.com

†Xonics@tongji.edu.cn

- [1] B. Li, L. Wang, and G. Casati, *Phys. Rev. Lett.* **93**, 184301 (2004).
- [2] C. W. Chang, D. Okawa, A. Majumdar, and A. Zettl, *Science* **314**, 1121 (2006).
- [3] E. Nefzaoui, K. Joulain, J. Drevillon, and Y. Ezzahri, *Appl. Phys. Lett.* **104**, 103905 (2014).
- [4] P. Ben-Abdallah and S.-A. Biehs, *Appl. Phys. Lett.* **103**, 191907 (2013).
- [5] S. Basu and M. Francoeur, *Appl. Phys. Lett.* **98**, 113106 (2011).
- [6] B. Li, L. Wang, and G. Casati, *Appl. Phys. Lett.* **88**, 143501 (2006).
- [7] L. Wang and B. Li, *Phys. Rev. Lett.* **99**, 177208 (2007).
- [8] L. Wang and B. Li, *Phys. Rev. Lett.* **101**, 267203 (2008).
- [9] C. Guarcello, P. Solinas, A. Braggio, M. Di Ventra, and F. Giazotto, *Phys. Rev. Applied* **9**, 014021 (2018).
- [10] V. Kubyskiy, S.-A. Biehs, and P. Ben-Abdallah, *Phys. Rev. Lett.* **113**, 074301 (2014).
- [11] J. Klaers, *Phys. Rev. Lett.* **122**, 040602 (2019).
- [12] N. Li, J. Ren, L. Wang, G. Zhang, P. Hänggi, and B. Li, *Rev. Mod. Phys.* **84**, 1045 (2012).
- [13] G. Chen, *Nanoscale Energy Transport and Conversion: A Parallel Treatment of Electrons, Molecules, Phonons, and Photons* (Oxford University Press, Cambridge, England, 2005).
- [14] E. Pop, *Nano Res.* **3**, 147 (2010).
- [15] M. O. Scully, *Phys. Rev. Lett.* **104**, 207701 (2010).
- [16] M. O. Scully, K. R. Chapin, K. E. Dorfman, M. B. Kim, and A. Svidzinsky, *Proc. Natl. Acad. Sci. U.S.A.* **108**, 15097 (2011).
- [17] D. Segal and A. Nitzan, *Phys. Rev. Lett.* **94**, 034301 (2005).
- [18] T. Ruokola and T. Ojanen, *Phys. Rev. B* **83**, 241404(R) (2011).
- [19] J. Ren and J.-X. Zhu, *Phys. Rev. B* **87**, 241412(R) (2013).
- [20] K. Joulain, J. Drevillon, Y. Ezzahri, and J. Ordóñez-Miranda, *Phys. Rev. Lett.* **116**, 200601 (2016).
- [21] K. Joulain, Y. Ezzahri, and J. Ordóñez-Miranda, *Z. Naturforsch.* **72**, 163 (2017).
- [22] E. Pereira, *Phys. Rev. E* **99**, 032116 (2019).
- [23] C. Kargı, M. T. Naseem, T. Opatrný, Ö. E. Müstecaplıoğlu, and G. Kurizki, *Phys. Rev. E* **99**, 042121 (2019).
- [24] J. Ordóñez-Miranda, Y. Ezzahri, and K. Joulain, *Phys. Rev. E* **95**, 022128 (2017).
- [25] B.-q. Guo, T. Liu, and C.-s. Yu, *Phys. Rev. E* **98**, 022118 (2018).

- [26] C. Wang, X.-M. Chen, K.-W. Sun, and J. Ren, *Phys. Rev. A* **97**, 052112 (2018).
- [27] B.-q. Guo, T. Liu, and C.-s. Yu, *Phys. Rev. E* **99**, 032112 (2019).
- [28] J. Du, W. Shen, S. Su, and J. Chen, *Phys. Rev. E* **99**, 062123 (2019).
- [29] Y. Zhang, X. Zhang, Z. Ye, G. Lin, and J. Chen, *Appl. Phys. Lett.* **110**, 153501 (2017).
- [30] F. Giazotto and M. J. Martínez-Pérez, *Nature (London)* **492**, 401 (2012).
- [31] A. Ronzani, B. Karimi, J. Senior, Y.-C. Chang, J. T. Peltonen, C. Chen, and J. P. Pekola, *Nat. Phys.* **14**, 991 (2018).
- [32] K.-Y. Fong, H.-K. Li, R.-K. Zhao, S. Yang, Y. Wang, and X. Zhang, *Nature (London)* **576**, 243 (2019).
- [33] J. P. Pekola and B. Karimi, *Rev. Mod. Phys.* **93**, 041001 (2021).
- [34] C. Timm, *Phys. Rev. Lett.* **98**, 070604 (2007).
- [35] M. Walschaers, J. Fernandez-de-Cossio Diaz, R. Mulet, and A. Buchleitner, *Phys. Rev. Lett.* **111**, 180601 (2013).
- [36] D. Manzano, *PLoS One* **8**, e57041 (2013).
- [37] N. Kulvelis, M. Dolgushev, and O. Mülken, *Phys. Rev. Lett.* **115**, 120602 (2015).
- [38] C. Maier, T. Brydges, P. Jurcevic, N. Trautmann, C. Hempel, B. P. Lanyon, P. Hauke, R. Blatt, and C. F. Roos, *Phys. Rev. Lett.* **122**, 050501 (2019).
- [39] M. Ehrhardt, R. Keil, L. J. Maczewsky, C. Dittel, M. Heinrich, and A. Szameit, *Sci. Adv.* **7**, eabc5266 (2021).
- [40] J. Thingna, D. Manzano, and J. Cao, *Sci. Rep.* **6**, 28027 (2016).
- [41] J. Thingna, D. Manzano, and J. Cao, *New J. Phys.* **22**, 083026 (2020).
- [42] J. Wu and J. Cao, *J. Chem. Phys.* **139**, 044102 (2013).
- [43] J. Schnakenberg, *Rev. Mod. Phys.* **48**, 571 (1976).
- [44] D. Andrieux and P. Gaspard, *J. Stat. Phys.* **127**, 107 (2007).
- [45] B. Altaner, S. Grosskinsky, S. Herminghaus, L. Katthän, M. Timme, and J. Vollmer, *Phys. Rev. E* **85**, 041133 (2012).
- [46] M. Einax and A. Nitzan, *J. Phys. Chem. C* **118**, 27226 (2014).
- [47] M. Einax and A. Nitzan, *J. Chem. Phys.* **145**, 014108 (2016).
- [48] G. T. Craven and A. Nitzan, *Phys. Rev. Lett.* **118**, 207201 (2017).
- [49] G. T. Craven and A. Nitzan, *J. Chem. Phys.* **146**, 092305 (2017).
- [50] G. T. Craven, D. H. He, and A. Nitzan, *Phys. Rev. Lett.* **121**, 247704 (2018).
- [51] Z. Zhang and J. Wang, *New J. Phys.* **17**, 043053 (2015).
- [52] S. Rahav, J. Horowitz, and C. Jarzynski, *Phys. Rev. Lett.* **101**, 140602 (2008).
- [53] V. Y. Chernyak and N. A. Sinitsyn, *Phys. Rev. Lett.* **101**, 160601 (2008).
- [54] D. Mandal and C. Jarzynski, *J. Stat. Mech.* (2011) P10006.
- [55] S. Asban and S. Rahav, *Phys. Rev. Lett.* **112**, 050601 (2014).
- [56] J. Ren, V. Chernyak, and N. Sinitsyn, *J. Stat. Mech.* (2011) P05011.
- [57] H. T. Quan, Y.-x. Liu, C. P. Sun, and F. Nori, *Phys. Rev. E* **76**, 031105 (2007).
- [58] G. Watanabe, B. P. Venkatesh, P. Talkner, and A. del Campo, *Phys. Rev. Lett.* **118**, 050601 (2017).
- [59] P. Abiuso and M. Perarnau-Llobet, *Phys. Rev. Lett.* **124**, 110606 (2020).
- [60] R. D. Mayrhofer, C. Elouard, J. Splettstoesser, and A. N. Jordan, *Phys. Rev. B* **103**, 075404 (2021).
- [61] D. Venturelli, R. Fazio, and V. Giovannetti, *Phys. Rev. Lett.* **110**, 256801 (2013).
- [62] N. Linden, S. Popescu, and P. Skrzypczyk, *Phys. Rev. Lett.* **105**, 130401 (2010).
- [63] L. A. Correa, J. P. Palao, G. Adesso, and D. Alonso, *Phys. Rev. E* **87**, 042131 (2013).
- [64] M. Poletini and M. Esposito, *J. Stat. Mech.* (2014) P10033.
- [65] M. Poletini, *Lett. Math. Phys.* **105**, 89 (2015).
- [66] J. A. Owen, T. R. Gingrich, and J. M. Horowitz, *Phys. Rev. X* **10**, 011066 (2020).
- [67] B. Rutten, M. Esposito, and B. Cleuren, *Phys. Rev. B* **80**, 235122 (2009).
- [68] U. Weiss, *Quantum Dissipative Systems* (World Scientific, Singapore, 2012), Vol. 13.
- [69] H.-P. Breuer, F. Petruccione *et al.*, *The Theory of Open Quantum Systems* (Oxford University Press on Demand, New York, 2002).
- [70] W. H. Zurek, *Phys. Rev. D* **24**, 1516 (1981).
- [71] See Supplementary Material at <http://link.aps.org/supplemental/10.1103/PhysRevLett.128.067701> for the derivation and calculation details, which includes Refs. [20,69,72,73].
- [72] B. Sothmann and M. Büttiker, *Europhys. Lett.* **99**, 27001 (2012).
- [73] S.-W. Li, C. Cai, and C. Sun, *Ann. Phys. (Amsterdam)* **360**, 19 (2015).
- [74] T. L. Hill and O. Kedem, *J. Theor. Biol.* **10**, 399 (1966).
- [75] T. L. Hill and Y.-D. Chen, *Proc. Natl. Acad. Sci. U.S.A.* **72**, 1291 (1975).
- [76] H.-H. Kohler and E. Vollmerhaus, *J. Math. Biol.* **9**, 275 (1980).
- [77] H. Qian, *Annu. Rev. Phys. Chem.* **58**, 113 (2007).
- [78] J. Wang, *Adv. Phys.* **64**, 1 (2015).
- [79] J. Ren, *Front. Phys.* **12**, 120505 (2017).
- [80] A. C. Barato and U. Seifert, *Phys. Rev. Lett.* **114**, 158101 (2015).
- [81] H. Qian, S. Kjelstrup, A. B. Kolomeisky, and D. Bedeaux, *J. Phys. Condens. Matter* **28**, 153004 (2016).
- [82] D.-Q. Jiang, M. Qian, and M.-P. Qian, *Mathematical Theory of Nonequilibrium Steady States: On the Frontier of Probability and Dynamical Systems* (Springer Science & Business Media, New York, 2004).
- [83] J. Ren, *Phys. Rev. B* **88**, 220406(R) (2013).
- [84] Y. Meir and N. S. Wingreen, *Phys. Rev. Lett.* **68**, 2512 (1992).
- [85] H. Haug and A. P. Jauho, *Quantum Kinetics in Transport and Optics of Semiconductors* (Springer, Berlin, 2007).
- [86] A.-M. Daré and P. Lombardo, *Phys. Rev. B* **96**, 115414 (2017).
- [87] N. Walldorf, A. P. Jauho, and K. Kaasbjerg, *Phys. Rev. B* **96**, 115415 (2017).
- [88] B. Karimi, J. Pekola, M. Campisi, and R. Fazio, *Quantum Sci. Technol.* **2**, 044007 (2017).